Thermocline Variability in Different Dynamic Regions

ZHENGYU LIU

Department of Atmospheric and Oceanic Sciences, University of Wisconsin-Madison, Madison, Wisconsin

(Manuscript received 20 May 1994, in final form 4 March 1996)

ABSTRACT

The response of thermocline circulation to a variable wind forcing is investigated with quasigeostrophic models. The physical mechanism responsible for the different variability features in various dynamic regions has been highlighted. Special attention is given to the role of density advection that is forced by wind-driven currents in affecting baroclinic thermocline variability. The strong density advection in the Rhines–Young pool can effectively balance the variability induced by local Ekman pumping, resulting in weak baroclinic variability in the pool zone. In contrast, the lack of density advection in the shadow zone enables the local Ekman pumping to force significant baroclinic variability there. The variability in the barotropic field and the western boundary current system is also discussed.

1. Introduction

Most previous studies of thermocline circulation have focused on its steady aspects (e.g., Rhines and Young 1982; Luyten et al. 1983). The temporal variability of thermocline circulation has rarely been investigated. On the other hand, observations have clearly identified basin-scale thermocline variability with timescales ranging from annual to interdecadal (Tabara et al. 1986; Roemmich and Wunsch 1984; Levitus 1988; Antonov 1993; Talley and White 1987; Qiu and Joyce 1992; Deser et al. 1996). At the same time, significant climate variability has also been observed in the surface wind and buoyancy flux forcing fields (e.g., Kushnir 1994; Deser and Blackmon 1993; Deser et al. 1996). Since the thermocline circulation is forced by surface wind and buoyancy fields, it is conceivable that a significant part of thermocline variability may be driven by the variations of the surface forcing fields.

Thermocline variability under annual and decadal wind forcings has been investigated in a simple ventilated thermocline model (Liu 1993a,b). One important finding is a dramatic difference of baroclinic variability between the ventilated zone and the shadow zone. Under a variable wind (but with a fixed surface buoyancy flux), baroclinic variability is much weaker in the ventilated zone than in the shadow zone. This seemingly surprising result is caused by the different dynamic natures between the two zones, which can be understood from the theory of steady thermocline circulation. Density variability is dominated by advection processes in the ventilated zone, but by baroclinic Rossby waves in the shadow zone. The former can adjust rapidly with the wind forcing due to the barotropic process, but the latter does not. It is this difference in dynamics that causes the different baroclinic variability between the two dynamical regions.

With the same physical argument, one may speculate a weaker thermocline variability in the Rhines–Young pool than in the shadow zone. This is because, as in the ventilated zone, the dynamics of the Rhines–Young pool is also dominated by advection processes at the lowest order (Rhines and Young 1982). This weak variability in the pool has been observed by Dewar (1989) in a 2-layer quasigeostrophic (QG) model. However, the physical mechanism has not been fully discussed.

Emphasis will be placed on the physical mechanisms that generate different thermocline variability between the pool zone and the shadow zone. The role of density advection in affecting thermocline variability will be highlighted. In addition to the classical mechanism of the planetary wave, it will be shown that density advection can play a significant role in affecting thermocline variability. Section 2 presents physical arguments to explain the different variability between the pool zone and the shadow zone. Supporting numerical experiments are carried out with a 2-layer QG model in section 3. A summary and discussion are given in section 4.

2. Different thermocline variability between the pool zone and the shadow zone

For the thermocline in the interior ocean, at the lowest order, the inviscid 2-layer QG equations can be written as

Corresponding author address: Zhengyu Liu, Department of Atmospheric and Oceanic Sciences, University of Wisconsin-Madison, Madison, WI 53706-1695.
E-mail: znl@meteor.wisc.edu

$$\partial_t q_1 + J(\psi_1, q_1) = \frac{f_0}{H} w_e(x, y, t) \qquad (2.1a)$$

$$\partial_t q_2 + J(\psi_2, q_2) = 0. \qquad (2.1b)$$

Here the upper- and lower-layer planetary geostrophic potential vorticities are respectively

$$q_1 = \beta y + (\psi_2 - \psi_1)/(2L_D^2)$$

$$q_2 = \beta y + (\psi_1 - \psi_2)/(2L_D^2).$$

The total depth of the model ocean is $2H$, where H represents the depth at the bottom of the thermocline. The thermocline is represented by a 2-layer fluid with equal depths H. The deformation radius is $L_D^2 = \gamma H/(2f_0^2)$ with γ being the reduced gravity. Other notations are standard. The relative vorticity is neglected because we are interested in the thermocline variability in the interior ocean at annual to decadal timescales. A weak downgradient potential vorticity dissipation, which is also crucial for the potential vorticity homogenization in closed geostrophic contours, is neglected in (2.1).

The barotropic response in the interior ocean is simple. Defining the barotropic streamfunction as $\psi_B = (\psi_1 + \psi_2)/2$, one can easily derive the Sverdrup relation from Eqs. (2.1a,b) as

$$\beta \partial_x \psi_B = f_0 w_e(x, y, t)/(2H). \qquad (2.2a)$$

This shows that the barotropic flow is in an instantaneous Sverdrup balance. Physically, the instantaneous adjustment is achieved by the rapid barotropic Rossby waves, which have been filtered out in (2.1) because relative vorticity is neglected. The instantaneous barotropic response assures a simple, linear barotropic response to a variable wind in the interior ocean as

$$\partial_x \psi_B' = f_0 \Delta w_e'(x, y, t)/(2H), \qquad (2.2b)$$

where $A' = A - \bar{A}$ is the deviation from the time mean, $\bar{A}$. Therefore, the barotropic variability is linearily proportional to the local variability of the Ekman pumping. This relation is dependent on neither the location nor the forcing frequency.

The interior baroclinic response is more complicated. We will discuss the variability in terms of its dynamical balance, following a similar argument of Liu (1993a) in the case of a ventilated thermocline. Defining the baroclinic streamfunction proportional to interface elevation η as $\psi_C = \psi_2 - \psi_1 \sim \eta$, one can subtract (2.1a,b) to give the evolution equation for the baroclinic flow as (Dewar 1989)

$$[\partial_t + (u_B + C)\partial_x + v_B \partial_y]\left(\frac{\psi_C}{L_D^2}\right) = \frac{f_0 w_e}{H}. \qquad (2.3)$$

Here $C = -\beta L_D^2$ is the planetary wave speed, and u_B and v_B are barotropic velocities determined by the instantaneous Ekman pumping according to Sverdrup relation (2.2a). Equation (2.3) states that, even in the case of a finite amplitude variability, the baroclinic anomaly propagates as a nondispersive planetary wave advected by the barotropic flow.

To see the physical mechanism for the baroclinic variability in different dynamic regions, the dynamical balance from Eq. (2.3) is first discussed in the case of a steady circulation. In the shadow zone, $\psi_2 = 0$ and therefore $\psi_B = \psi_1/2$ and $\psi_C = -\psi_1$. Thus, advection vanishes and Eq. (2.3) degenerates to

$$C\partial_x\left(\frac{\psi_C}{L_D^2}\right) = \frac{f_0 w_e}{H}, \quad \text{shadow zone.} \qquad (2.4)$$

This states that the forcing from Ekman pumping is completely balanced by baroclinic Rossby waves. For example, in a subtropical gyre, a downward Ekman pumping tends to warm (deepen) the thermocline. This is balanced by the cooling (shoaling) due to the eastward planetary wave propagation of the thermocline interface that deepens toward the west.

In the pool zone, the lower layer potential vorticity is homogenized, or $q_2 = \beta y + \psi_C/(2L_D^2) \equiv$ const. Therefore, ψ_C is independent of longitude or $\partial_x \psi_C = 0$, and the steady form of Eq. (2.3) collapses to

$$v_B \partial_y\left(\frac{\psi_C}{L_D^2}\right) = \frac{f_0 w_e}{H}, \quad \text{pool zone.} \qquad (2.5)$$

Opposite to the shadow zone in (2.4), the forcing from Ekman pumping is completely balanced by density advection. Thus, in a subtropical gyre, the downward warm (deepening) tendency caused by Ekman pumping is opposed by the cold advection from the north due to the southward Sverdrup flow. This dynamical balance is similar to the ventilated zone in Liu (1993a).

A significant difference in the dynamical balance between the pool zone and the shadow zone in the steady thermocline has been seen. The pool zone is dominated by advection, while the shadow zone is dominated by planetary waves. It will further be seen that this difference results in dramatically different baroclinic thermocline variability. Indeed, if the temporal thermocline variability is considered, a qualitative difference between the dynamical balances of the shadow zone (2.4) and the pool zone (2.5) should be noted. The shadow zone is determined purely by the baroclinic process, while the pool zone involves the barotropic response. The consequence of this dynamical difference on thermocline variability can be understood in the following thought experiment. Imagine that the thermocline is initially in a steady state as in (2.4) and (2.5). Suddenly, the Ekman pumping is changed to a new Ekman pumping. How does the thermocline adjust to establish the new steady state?

In the shadow zone the steady balance of (2.4) can no longer hold. This is because the adjustment of baroclinic waves from the eastern boundary is very slow, and therefore initially the planetary wave term $\beta \partial_x \psi_C$ remains almost unchanged. Consequently, the anoma-

lous Ekman pumping is balanced mostly by the local variability

$$\partial_t \psi_C' \approx \frac{f_0 w_e'}{H} \neq 0. \tag{2.6}$$

In other words, strong baroclinic variability will be generated.

In sharp contrast, in the pool zone a new balance is achieved instantaneously between the new advection and the new Ekman pumping. This occurs because after the sudden change of Ekman pumping, the barotropic velocity responds to the new Ekman pumping immediately according to the instantaneous Sverdrup relation (2.2a). This rapid barotropic response enables a new balance like (2.5) to be reestablished before any change in the baroclinic flow, ψ_C. In other words, the anomalous Ekman pumping is balanced immediately by the anomalous advection

$$v_B' \partial_x \psi_C = \frac{f_0 w_e'}{H}, \tag{2.7}$$

and therefore

$$\partial_t \psi_C = 0.$$

This thought experiment explains why baroclinic variability should be much weaker in the pool zone than in the shadow zone. It is the difference between the dynamical natures of the two regions that results in the dramatically different baroclinic response. In the shadow zone, density advection is weak and the baroclinic variability is easily excited by local Ekman pumping and baroclinic Rossby waves. However, in the pool zone, the density advection is dominant. The dominant advection, along with a rapid barotropic adjustment process, results in the baroclinic variability being unnecessary.

Dewar (1989) points out that the weak baroclinic variability in the pool zone is due to the lack of baroclinic Rossby waves within the homogeneous potential vorticity pool. However, it remains unclear how variable Ekman pumping is balanced. The present study shows that variable Ekman pumping plays dual roles in the pool zone. First, it provides a variable forcing from Ekman pumping of the thermocline; second, it generates a variable barotropic flow and an associated density advection. Since the barotropic flow responds instantaneously to the variable Ekman pumping, the density advection due to barotropic flow exactly balances the variable Ekman pumping. Thus, there is no thermocline variability within the pool zone. Furthermore, this explanation predicts a similarity of thermocline variability between the pool zone and the ventilated zone: both regions are dominated by density advection, and therefore have weak baroclinic variability. In contrast, the shadow zone is dominated by planetary waves and therefore has a strong thermocline variability.

3. Numerical results

To verify the above speculation, numerical experiments are carried out in a 2-layer full QG model:

$$\partial_t q_1 + J(\psi_1, q_1) = \frac{f_0}{H} w_e + d\nabla^2 q_1 \tag{3.1a}$$

$$\partial_t q_2 + J(\psi_2, q_2) = d\nabla^2 q_2, \tag{3.1b}$$

where the upper and lower layer potential vorticities are respectively

$$q_1 = \beta y + \nabla^2 \psi_1 + (\psi_2 - \psi_1)/(2L_D^2)$$

$$q_2 = \beta y + \nabla^2 \psi_2 + (\psi_1 - \psi_2)/(2L_D^2).$$

Other notation is the same as in Eqs. (2.1a,b). The model domain is a 2000 km × 2000 km square basin with a free-slip lateral boundary condition. The parameters in the experiments are chosen as $2H = 1000$ m and $\gamma = 1$ cm s^{-2}. The equations are solved with a leapfrog time stepping. A FFT elliptical solver is used to derive streamfunctions from potential vorticities. The spatial resolution is about 15 km × 30 km. The dissipation coefficient is taken as $d = 3 \times 10^6$ cm^2 s^{-1}. A sponge layer is added along the western boundary, in which the viscosity is increased linearly from 100 km away from the boundary to the value of $d = 3 \times 10^7$ cm^2 s^{-1} on the western boundary. The addition of the sponge layer is purely for illustrative purposes and does not qualitatively change the conclusions.

The Ekman pumping takes a double gyre pattern: $w_e(y, t) = W_0(t) \sin[2\pi(y - y_0)/L]$, with the meridional model domain being $(-L/2, L/2)$, where $L = 2000$ km. Here $W_0(t)$ represents the amplitude of the Ekman pumping. Since the forcing is symmetric about the intergyre boundary at ($y_0 = 100$ km), the subtropical gyre is slightly larger than the subpolar gyre.

The steady circulation after 10 years of integration is presented in Fig. 1. The strength of the Ekman pumping is taken as $W_0 = \bar{W}_0 = 0.5 \times 10^{-4}$ cm s^{-1}. In the interior ocean, the most visible feature is a large Rhines–Young pool with a homogeneous lower-layer potential vorticity (Fig. 1f), within which the lower layer has a significant circulation (Fig. 1b). The baroclinic streamfunction (Fig. 1d) shows a flow pattern different between the pool zone and the shadow zone. The zonal gradient is strong in the shadow zone, but almost vanishes in the pool zone. The latter is expected from the potential vorticity homogenization because the baroclinic flow associated with the vorticity stretching balances the planetary vorticity. In the western boundary layer, despite the sponge layer, a pair of inertial recirculations exist, each of which has a strong barotropic core (Figs. 1a–d).

With the flow in Fig. 1 as the initial state, an annual variable wind is started with an amplitude of 50% of the mean, that is, $W_0(t) = \bar{W}_0[1 + 0.5 \sin(\omega t)]$, where ω represents the annual frequency. This amplitude

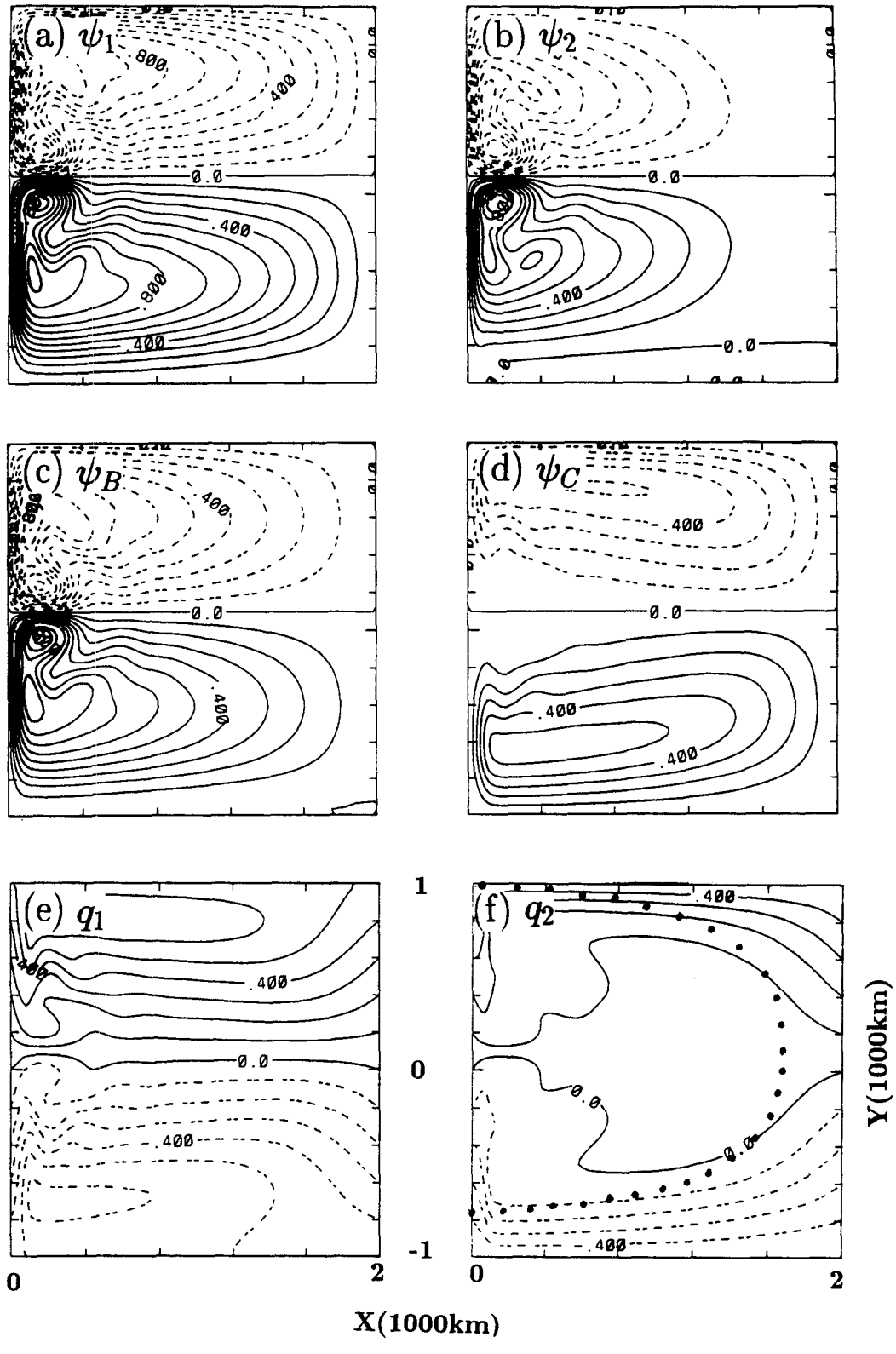

FIG. 1. Steady circulation of the double gyre under the mean wind forcing: (a) Upper layer streamfunction, (b) lower layer streamfunction, (c) barotropic streamfunction, (d) baroclinic streamfunction, (e) upper layer potential vorticity, and (f) the lower layer potential vorticity. The contour interval is 10^7 cm^2 s^{-1} for the streamfunctions and $\beta \times 100$ km for the potential vorticities. In (f), the dotted line represents the boundary of the pool calculated from the outmost closed geostrophic contour $\beta y + \psi_B/L_D^2$.

roughly corresponds to the observed wind variation (Levitus 1988). After switching to the annual wind for several years, the flow field settles into a regular annual cycle, upon which the following analysis is based. The annual mean flow (not shown) virtually resembles the initial state in Fig. 1.

a. Barotropic variability

The annual variability of the barotropic flow is calculated as $\psi'_B(x, y, t) = \psi_{Ba}(x, y) \sin[\omega t - \theta(x, y)]$, where $\psi_{Ba}(x, y)$ and $\theta(x, y)$ are the amplitude and phase, respectively (Figs. 2a and 2c). In the interior ocean, as predicted by the instantaneous Sverdrup relation (2.2a,b), the pattern of the barotropic variability resembles that of the mean flow in Fig. 1c, and the phase has a zero lag. Furthermore, the response is very linear as shown in Fig. 2e, which presents the ratio of the amplitude of the annual harmonic to that of the total variability. The annual variability accounts for more than 90% of the variability over most of the domain.

This simple variability pattern is changed modestly in the western boundary current/inertial recirculation system. Especially near the recirculation cell the phase lag can reach up to 3 months. It is somewhat surprising (see Fig. 2e) that the strongest reduction of annual harmonics occurs not within the recirculation cells where the nonlinear advection of relative vorticity is the strongest, but occurs in the region between the recirculation cells and the interior pool zone where the variability accounted for by the annual component reduces to below 20%. This point will be revisited.

b. Baroclinic variability

The baroclinic variability is shown in Figs. 2b,d,f. The amplitude pattern in Fig. 2b clearly shows three regions of baroclinic variability, with the strongest in the western boundary/inertial recirculation region, the intermediate in the shadow zone, and the weakest in the pool zone.

The most striking feature in the interior ocean is a much weaker variability in the pool zone than in the shadow zone. This feature agrees with previous physical arguments in section 2. To highlight the physics, the evolution of each term of the potential vorticity equation for the baroclinic flow is further plotted. The equation is derived by subtracting (3.1a) and (3.1b) as

$$[\partial_t q_C] + [J(\psi_1, \nabla^2\psi_1) - J(\psi_2, \nabla^2\psi_2)] + [J(\psi_B, \psi_C/L_D^2)] + [\beta\partial_x\psi_C] = [f_0 w_e/H] + [d\nabla^2 q_C], \quad (3.2)$$

where $q_C \equiv q_1 - q_2$.

In the shadow zone, Fig. 3b presents an example of the evolution of each term in Eq. (3.2). For the time-mean dynamic balance, the wind stress is balanced by the β term (or the Rossby wave) as expected in Eq. (2.4). For the variability part, the dominant term is a local balance of $\partial_t q'_C = f_0 w'_e/H$ as expected from (2.6). For lower frequencies, the effect of the Rossby wave term $\beta\partial_x\psi'_C$ would also become important, but the advection term is always negligible. Thus, as expected from (2.6), the variable wind can force significant local variability in the shadow zone because of the slow adjustment of the baroclinic Rossby waves, and the absence of the advective process.

The pool zone dynamics shows a sharp contrast to that of the shadow zone. The example in Fig. 3a shows clearly that for both the time-mean and perturbation, the dominant dynamical balance is the advection and local Ekman pumping as in Eqs. (2.5) and (2.7). The local variability remains small during the whole annual cycle, as is expected from Eq. (2.7). Thus, the dominant advection, together with the rapid adjustment of the barotropic current with the anomalous Ekman pumping [see (2.2a,b)], suppresses the baroclinic variability in the pool zone.

In the western boundary current system, a closer examination of Fig. 2b shows three small subregions of maximum baroclinic variability: the western boundary, the inertial recirculation cell, and the connection region between the recirculation cell and the pool zone. This multiple maximum pattern differs dramatically from the barotropic variability, which has a single maximum in the recirculation cell (Fig. 2a). Further experiments indicate that these variability features are independent of the sponge layer.

The three regions of variability can also be identified clearly in the phase diagram of the baroclinic variability in Fig. 2d. In the shadow zone, the variability lags the local Ekman pumping by about 3 months, as expected from the local response (2.6). The westward propagation of the Rossby wave is not present except near the eastern boundary. This is because the annual forcing is too fast to generate strong baroclinic waves. The phase also exhibits a rapid transition downstream along the western boundary current and eventually circulates back into the pool zone, indicating a strong influence on the pool zone by the penetration of boundary currents.

Overall, the baroclinic response is nearly linear in the interior ocean (Fig. 2e) because of its small amplitude under the annual forcing, which is much higher than the baroclinic waves (Liu 1993b). However, the strong nonlinearity implied by the reduction of the amplitude of the annual harmonic relative to the total variability occurs between the recirculation cell and the pool zone. This region of nonlinearity corresponds well to that in the barotropic variability (Fig. 2e) and therefore seems to be caused by barotropic–baroclinic interactions. There is also an indication of nonlinearity along the boundary between the pool zone and shadow zone. This point will be revisited later.

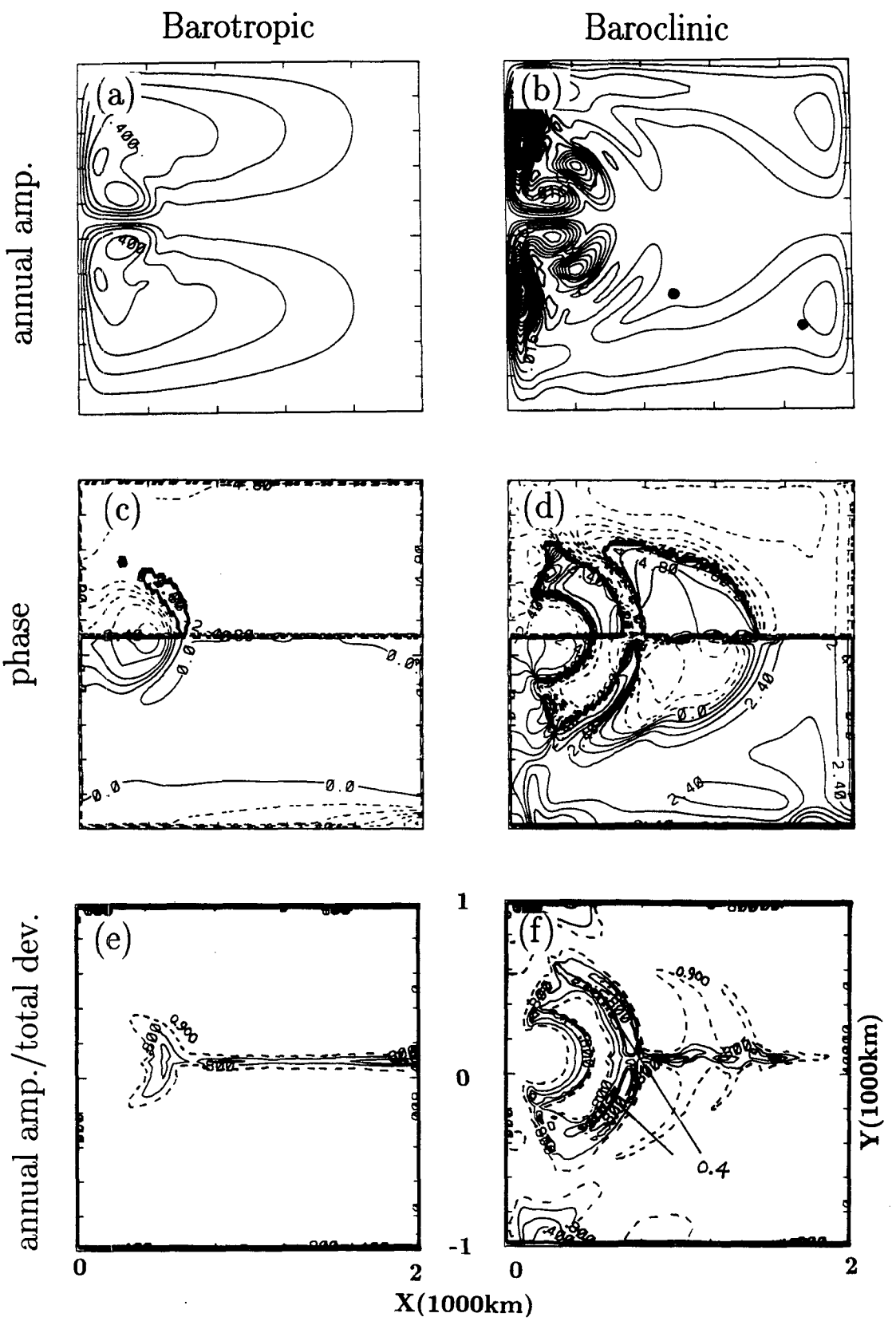
Barotropic
Baroclinic
annual amp.
phase
annual amp./total dev.
(a)
(b)
(c)
(d)
(e)
(f)
0.4
1
0
-1
0
2
0
2
X(1000km)
Y(1000km)

c. Variability in deep thermocline circulation

As shown in Fig. 2a, a strong barotropic variability occurs within the entire basin. This feature will significantly affect the lower-layer flow, particularly in the shadow zone where the mean advection is weak. This is illustrated in Fig. 4, which presents three snapshots of lower layer flow from winter to summer. In winter (Fig. 4a), the subtropical gyre (Fig. 4a) has stronger-than-normal Ekman pumping (downwelling) that produces an anomalous southward barotropic flow according to (2.2b). In the shadow zone where the mean flow is absent, this anomalous flow appears as a southward flow, expanding the anticyclonic gyre to the entire basin. In contrast, in summer (Fig. 4c), the weaker-than-normal Ekman pumping downwelling produces a northward anomalous barotropic flow that produces a northward flow in the shadow zone, which returns in the pool zone. Therefore, a cyclonic gyre appears in the shadow zone, producing a lower layer flow pattern with two counterrotating gyres. During the transitional spring season, the flow in the shadow zone nearly vanishes (Fig. 4b). This lower-layer circulation variability is consistent with the analytical study of Liu (1993a,b) in a model of a ventilated thermocline.

d. Decadal forcing case

The decadal forcing effect can be seen in Fig. 5, which is exactly the same as shown in case Fig. 2, except for a decadal frequency forcing. In the interior ocean, the variability features are similar to the annual forcing case for both barotropic and baroclinic flows. In particular, the baroclinic variability is much weaker in the pool zone than in the shadow zone. This is not surprising because the physical arguments in section 2 do not depend crucially on the forcing frequency. Indeed, in the limit of very low frequency Ekman pumping, the difference of baroclinic variability features between the pool zone and shadow zone can be demonstrated analytically by using the classical Rhines–Young pool zone solution (Rhines and Young 1982).

Nevertheless, comparison with the annual case in Fig. 2 also shows some significant differences. The baroclinic variability is reduced substantially in the boundary current system (Fig. 5b) compared with the annual case in Fig. 2b. With a further reduction in the forcing frequency, the baroclinic variability will be reduced further in the western boundary system, and eventually the variability in the shadow zone becomes the strongest over the entire basin (not shown). In part, the reduction of the baroclinic variability in the recirculation region can be explained in terms of the lack of a baroclinic structure in the core of the recirculation cell in the steady circulation (Fig. 1d).

Finally, the nonlinearity is much stronger even in the interior ocean (Fig. 5f). In addition to the region between the recirculation cell and the pool zone, there is clearly another band of strong nonlinearity in the region between the pool zone and the shadow zone. Thus, for both barotropic and baroclinic variability, the strongest nonlinearity seems to occur in the boundary regions between two different dynamic regions. In addition, the strongly nonlinear regions are usually associated with regions of rapid phase transition, as seen by comparison of Fig. 2c with 2e, Fig. 2d with 2f, Fig. 5c with 5e, and Fig. 5d with 5f. The result here is reminiscent of the study of a ventilated thermocline, where the strongest baroclinic response occurs between the shadow zone and the ventilated zone—the so called Alternate Zone (Liu 1993a,b).

We may gain a better understanding of the complex dynamics in the region between two different dynamical regions in terms of the concept of Alternate Zone of Liu (1993a,b). The Alternate Zone is the region where the boundary between two dynamical regions (such as pool zone and shadow zone, or recirculation cell and pool zone) sweeps across under a varying wind forcing. In other words, a point within the Alternate Zone is alternatively located within two different dynamical regions during one period of variation. Thus, the Alternate Zone has two dramatically different dynamics during one period of variation. Furthermore, the difference between the dynamics of two regions usually is associated with different nonlinear advection process. For example, the shadow zone has no advection process; the pool zone is dominated by density advection but not relative vorticity (momentum) advection; recirculation is dominated by relative vorticity advection. Thus, it is conceivable that the dynamics in an Alternate Zone is very nonlinear. This explanation is consistent with the fact that the band of nonlinearity between the shadow zone and the pool zone is much clearer in the decadal case (Fig. 5f) than in the annual case (Fig. 2f) because the decadal forcing produces a much larger amplitude change in the shadow zone boundary. This change results in a large Alternate Zone (see Liu 1993a,b) and therefore stronger nonlinearity. The boundary of the recirculation cell, on the other hand, is related to the advection process of vorticity,

FIG. 2. The amplitude of the annual variability under the annual Ekman pumping: the amplitude of the barotropic (a) and baroclinic (b) anomaly, the phase of the barotropic (c) and baroclinic (d) anomaly, the ratio of the amplitude of the annual harmonic to that of the total variability for the barotropic (e) and baroclinic (f) flows. The contour interval for the amplitude is 10^7 cm^2 s^{-1} for (a), 0.04×10^7 cm^2 s^{-1} for (b), 0.6 month for (c) and (d), and 0.2 for (e) and (f). The contour interval 0.9 is also plotted on (e) and (f) as dashed curves. The two black dots on (b) show the positions on which the evolution of the dynamic balances are plotted in Fig. 3.

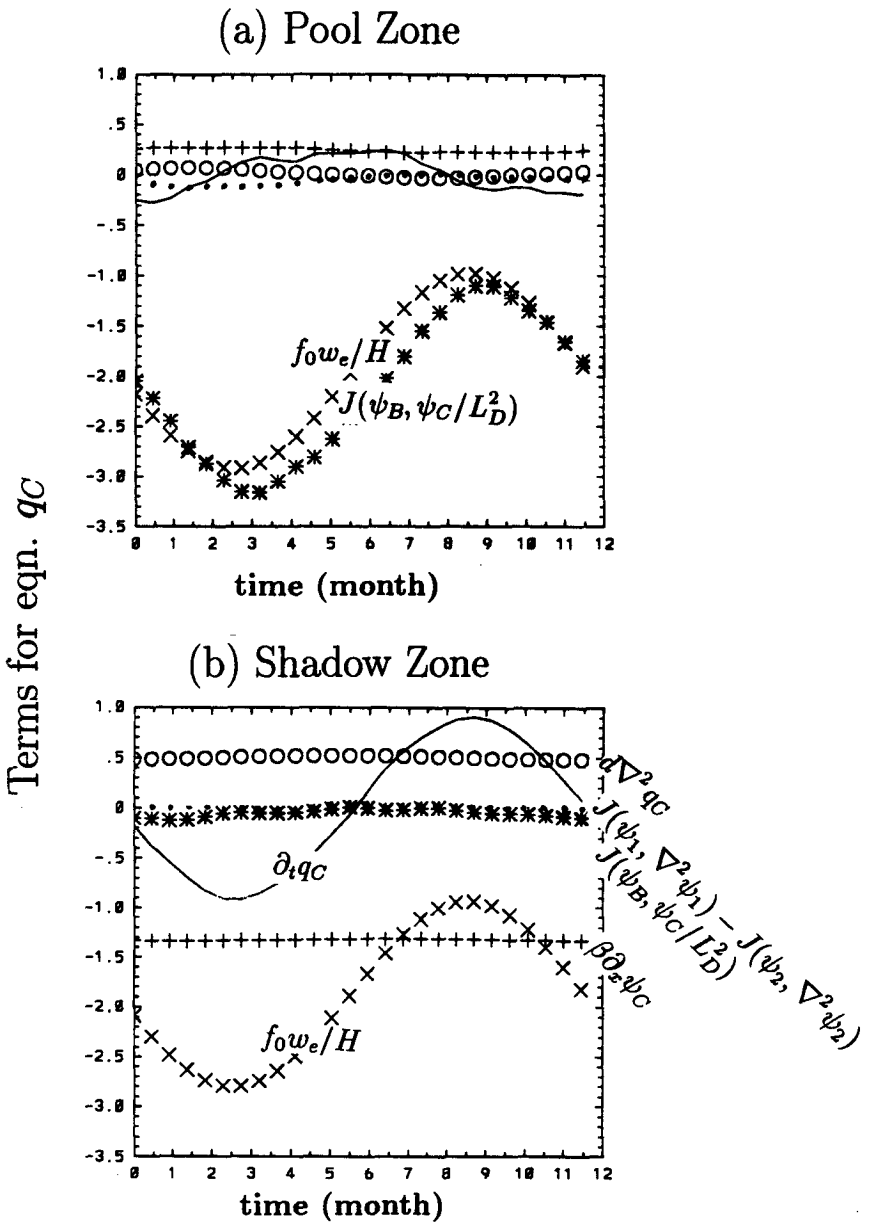

FIG. 3. The annual evolution of each term of the baroclinic equation (3.3) for a small area within the pool zone centered at (990 km, −330 km) (a) and within the shadow zone centered at (1830 km, −510 km), as marked by the two heavy dots in Fig. 2b. The curves are denoted [as in panel (b)] as $\partial_t q_C$ (solid), $J(\psi_1, \nabla^2\psi_1) - J(\psi_2, \nabla^2\psi_2)$ (dot), $J(\psi_B, \psi_C/L_D^2)$ (star), $\beta\partial_x\psi_C$ (plus), $f_0 w_e/H$ (cross), and $d\nabla^2 q_C$ (circle). The unit is arbitrary. The advection is important in the pool zone for both the mean and the variability part, producing little local baroclinic variability. In contrast, the absence of the advection in the shadow zone allows a significant local baroclinic variability.

which is a rather faster process (a year or so; Liu 1996). Thus, even under an annual forcing, the boundary of the recirculation cell can change substantially to generate a large Alternate Zone and in turn nonlinearity. Clearly, much study is needed for a further understanding of the dynamics of the Alternate Zone and its relation to thermocline variability.

4. Summary and discussion

Thermocline variability in a 2-layer QG model, with emphasis on the difference in the baroclinic variability between the pool zone and the shadow zone, has been investigated. It is found that the baroclinic variability is much weaker in the pool zone than in the shadow

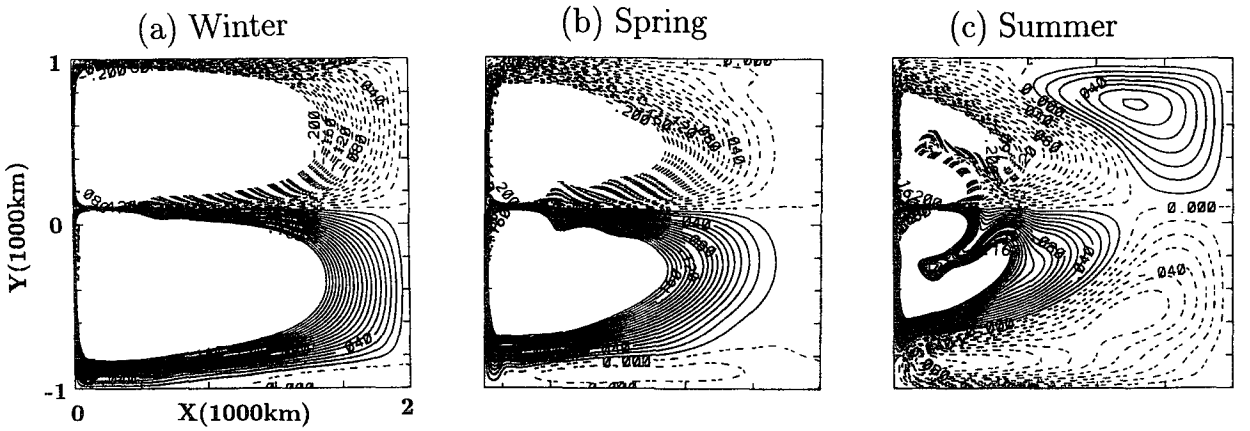

FIG. 4. The streamfunction of the lower layer circulation for winter (a), spring (b) and summer (c). The contour interval is 10^6 cm^2 s^{-1} and the contour values above 2×10^7 cm^2 s^{-1} are not plotted. In winter, the circulation exhibits an expanded anticyclonic circulation with southward flow in the shadow zone; in summer, two counterrotating gyres coexist in each gyre with a northward flow in the shadow zone.

zone. Physically this occurs because the density field is determined mainly by the advection process in the pool zone, but by baroclinic Rossby waves in the shadow zone. Therefore, in the pool zone the rapid adjustment of the barotropic flow results in a rapid adjustment of the density advection, generating weak baroclinic variability. In addition, the boundary region between two different dynamical regions tends to have a stronger nonlinearity and sharp phase transition in the variability. All these factors indicate that thermocline variability can be much better understood in terms of various dynamical regions.

In the past, local wind variations (Ekman pumping) and baroclinic Rossby waves are believed to be the two main mechanisms that produce basin-scale variability in the permanent thermocline (e.g., Anderson and Gill 1975; Mysak 1983; Emery and Magaard 1976; Price and Magaard 1980, 1983, 1986; White and Tabara 1987). This study highlights a new mechanism: the density advection. Indeed, density advection plays a crucial role in both modern thermocline theories (Rhines and Young 1982; Luyten et al. 1983). Without advection, neither a Rhines–Young pool nor a ventilated zone would exist! Thus, it is not surprising that advection also plays an important role in thermocline variability.

Several further issues are worth discussing.

a. Vertical resolution

Variability in a 2-layer model only has been discussed because the 2-layer model highlights the physical mechanisms most clearly. What happens with an increased vertical resolution? With more than two active layers, it is no longer possible to distinguish the density advection from the baroclinic planetary waves as clearly as in the 2-layer case of Eq. (2.3). However, since density advection is still the dominant mechanism in the pool zone, the baroclinic variability in the pool zone is still expected to be weaker than in the shadow zone because of the effective balance by the density advection of the local Ekman pumping effect. This has been confirmed in our QG experiments in a 3-layer model [by adding one more layer to Eqs. (3.1a,b)] (not shown, but relevant figures are shown in Figs. 6 and 7).

Here a quick way of understanding the variability in the 3-layer model is presented. In the limit of very low frequency forcing, the solution can be approximated by the steady circulation solution of Rhines and Young (1982). For the simple case of equal depth in each layer, their 3-layer solutions [their Eqs. (3.9), (3.11), and (3.12)] yield the interface elevation between layer 1 and layer 2 ($\eta = \psi_2 - \psi_1$) as

$$\eta_{S2} = \psi_B, \quad \text{shadow zone} \tag{4.1a}$$

$$\eta_{P2} = \frac{\psi_B}{3} + C_1 y, \quad \text{layer 2 pool zone} \tag{4.1b}$$

$$\eta_{P3} = C_2 y. \quad \text{layer 3 pool zone,} \tag{4.1c}$$

where $\psi_B \sim \int^x w_e(x, y, t)dx$ is the barotropic streamfunction, C_1 and C_2 are two constants, and a common factor has been neglected in (4.1a–c). The bottom friction has also been neglected [which only affects the solution in (4.1c)]. For a temporal variation of Ekman pumping Δw_e, the corresponding interface variation is

$$\Delta\eta_{S2} = \Delta\psi_B, \quad \text{shadow zone} \tag{4.2a}$$

$$\Delta\eta_{P2} = \frac{\Delta\psi_B}{3}, \quad \text{layer 2 pool zone,} \tag{4.2b}$$

$$\Delta\eta_{P3} = 0. \quad \text{layer 3 pool zone.} \tag{4.2c}$$

Thus, baroclinic variability is the strongest in the shadow zone, significantly weaker in the layer 2 pool

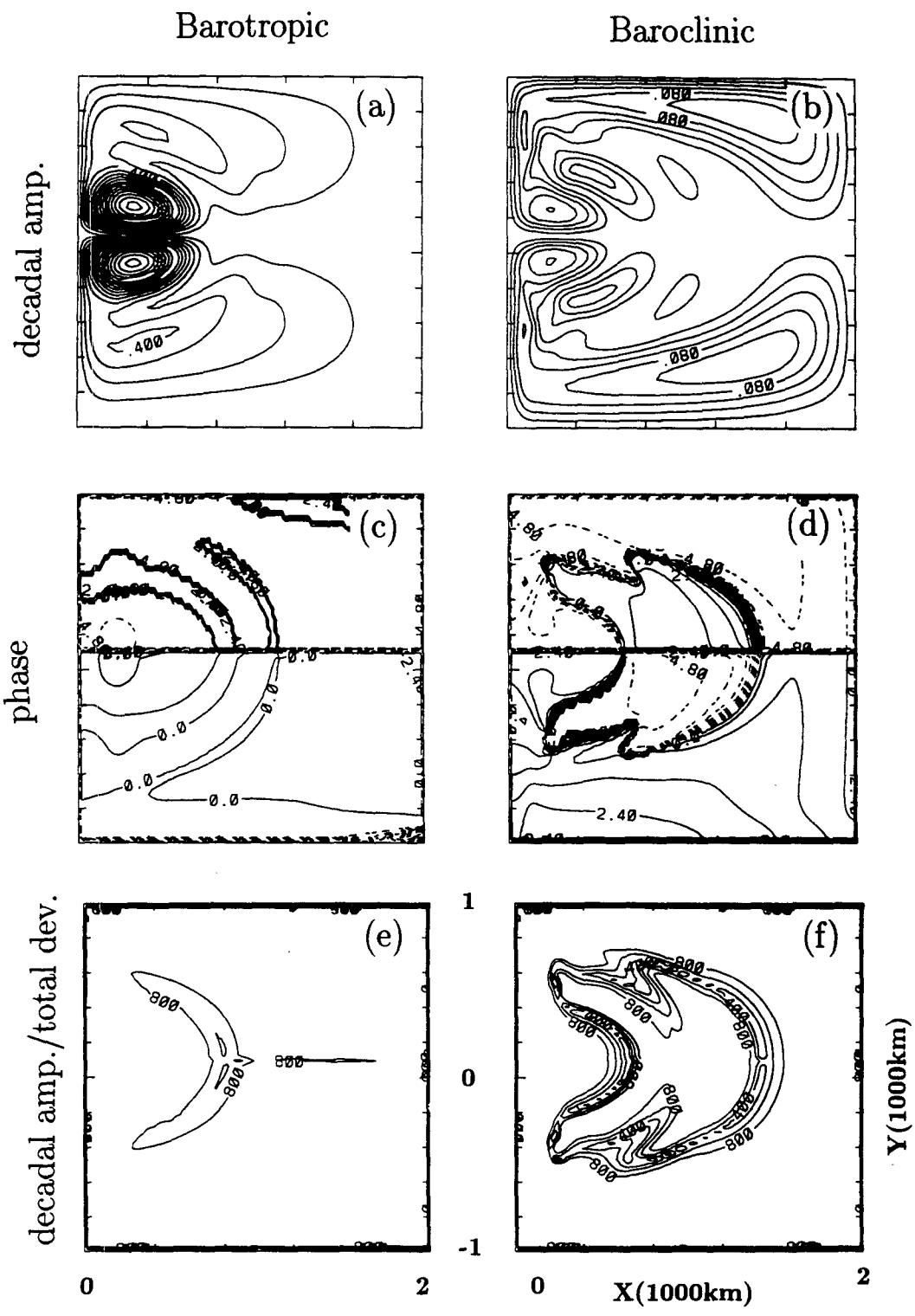

FIG. 5. As in Fig. 2, except for a decadal frequency. In (b), the contour interval is 0.2×10^7 cm^2 s^{-1}. In (c) and (d), the contour interval is now 0.6 year.

zone (outside the layer 3 pool), and vanishes in the layer 3 pool zone. With higher vertical resolution, we speculate that our general conclusion of a weaker variability in the pool zone should still hold, although a more detailed study is probably needed.

b. Eddy effect

The Rhines–Young pool is dominated by eddy activity, which results in the homogenization of the potential vorticity. In the QG model experiment (3.1) and the analytical solution (4.1), the eddy is parameterized as a constant coefficient downgradient diffusion of potential vorticity. However, eddy-resolving model studies show that, although the downgradient Q flux is more or less correct (after removing a quasi-rotational part), the mixing coefficient is not a constant (Marshall 1984; Holland and Rhines 1980). Thus, an eddy-resolving model experiment with a 3-layer QG model was carried out. Instead of using a Laplacian diffusion of potential vorticity with a constant mixing coefficient, a biharmonic mixing is used for streamfunctions in each layer. Thus, the mixing of potential vorticity in the model will be mainly carried by the eddies explicitly. (Other model parameters are listed in Table 1). A control run was performed under a steady wind forcing, which has a maximum wind stress of $\tau = 1$ dyn cm^{-2} in the middle of the basin. The potential vorticity in layer 2 and the interface between layer 1 and layer 2 are plotted in Fig. 6a and 6b for the statistically mean steady state. The homogenized potential vorticity pool is seen clearly in layer 2. To see the variability in the case of low-frequency forcing, another experiment was carried out with the same wind but with a reduced amplitude of 30%. The difference of the interface (between layer 1 and layer 2) for the two runs are plotted in Fig. 7. One sees clearly a weak variability tongue in the pool region. Deep inside the pool, however, the variability reaches its maximum because of the eddy activity and the variability of the recirculation. The submaximum of variability occurs in the shadow zone. The picture is qualitatively similar to the 2-layer model experiments in Fig. 2b and Fig. 5b. The weak variability tongue in the pool zone is, however, not as salient as in the 2-layer model. This is expected from the analytical argument of (4.2).

TABLE 1. Parameters for the eddy-resolving 3-layer QG model.

Basin domain	4000 km × 4000 km
Layer thickness	300 m, 700 m, 4000 m
Reduced gravity	$g_{12} = .03$ m s^{-2} $g_{23} = .02$ m s^{-2}
Coriolis parameter	$f_0 = 9.3 \times 10^{-5}$ s^{-1} $\beta = 2 \times 10^{-11}$ m^{-1} s^{-1}
Bihamonic dissipation coeff.	9×10^9 m^4 s^{-1}
Bottom friction coeff.	1×10^{-7} s^{-1}
resolution	25 km × 25 km
time step	2 h

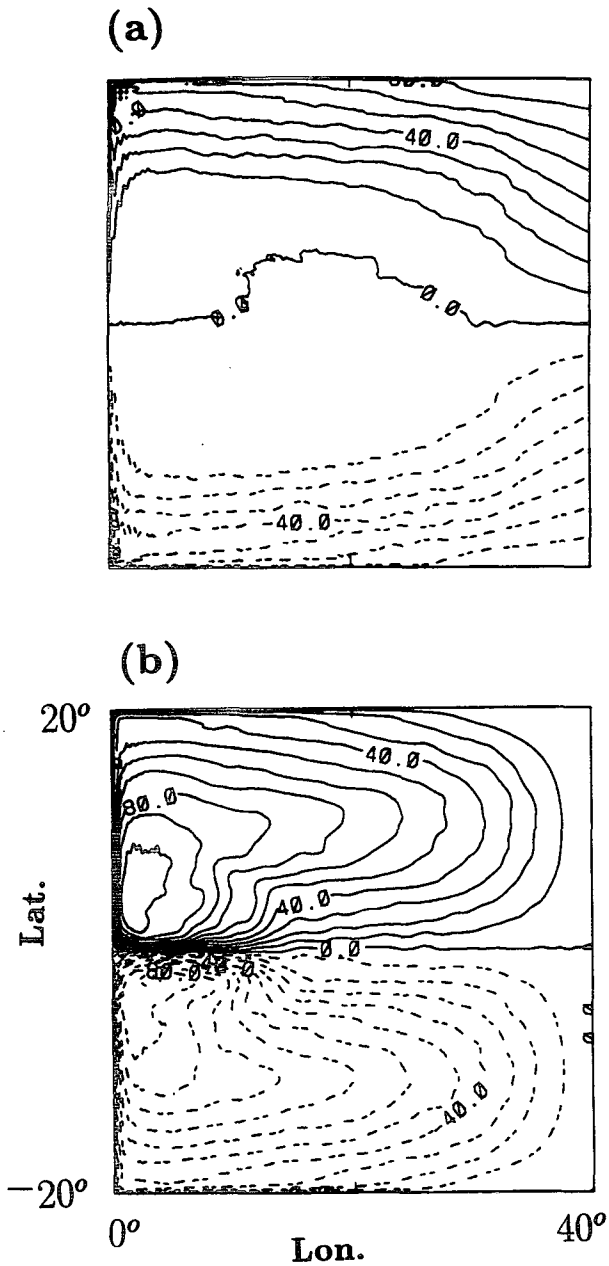

FIG. 6. Mean pattern in the eddy-resolving 3-layer QG model (with parameters in Table 1). The figure shows a 10-year time-mean pattern of (a) the second layer potential vorticity and (b) the interface between layer 1 and layer 2 (contour interval 20 m) (negative means deeper). The homogenized potential vorticity field is clearly seen.

Figure 7 seems to suggest that, with both eddy activity and increased vertical resolution, the Rhines–Young pool still exhibits a weaker baroclinic variability. However, further experiments with oscillating wind forcings seem to indicate that the feature of a weaker pool zone baroclinic variability becomes even less clear, even with a forcing frequency as low as $^1/_{10}$-year.

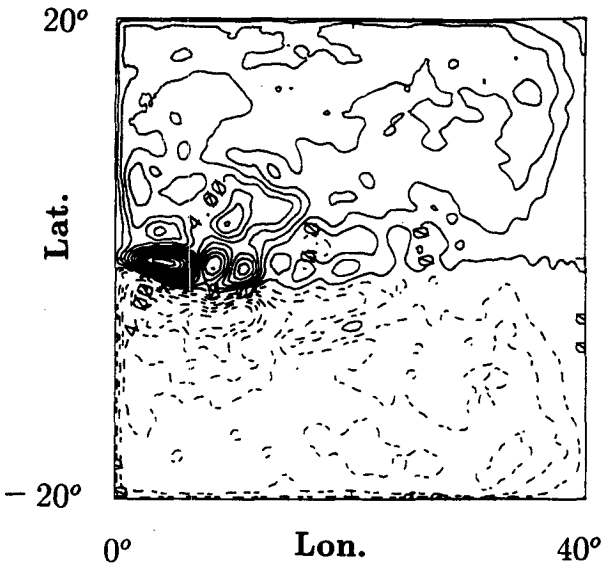

FIG. 7. The difference of layer interface between layer 1 and layer 2 for the run in Fig. 6 and a similar run but with a magnitude of wind reduced by 30%. The contour interval is 8 m. The weaker variability tongue in the outflank of the pool zone is visible. The recirculation region has the strongest variability, while the shadow zone has the second submaximum of variability.

Further study is needed to clarify this issue. This result may partly be caused by the long-term internal variability of the eddies and the associated wave-mean flow interaction. It may also be caused by the interaction between the internal and external variability. In any case, this seems to suggest that the parameterization of eddies will have a significant impact on the variability of large-scale ocean circulation.

c. *Western boundary current system*

Although this discussion has focused on the interior ocean, the boundary current/inertial recirculation system is also found to exhibit many distinctive variability features. However, the physical mechanisms remain to be understood.

d. *Migrating wind forcing*

We have only discussed the variability of wind forcing due to its change of amplitude. However, the wind forcing also exhibits strong variability in its spatial pattern. In particular, there is a migration of the wind pattern over certain meridional distances. Further studies show that an annual wind migration can significantly alter the thermocline variability features when compared to thermocline variability caused by the standing oscillating wind (not shown).

e. *Variable surface buoyancy forcing*

Just like the surface wind, the surface buoyancy flux can also produce strong baroclinic thermocline variability, with strong regional features due to a variable surface buoyancy flux forcing (Liu and Pedlosky 1994). Opposite to the variable surface wind, the variable surface buoyancy flux can change the subduction potential vorticity that tends to produce strong baroclinic variability in the ventilated zone, but not in the shadow zone. With the same argument, it seems reasonable to speculate that a surface buoyancy flux will not produce strong baroclinic variability in the Rhines–Young pool either. This follows because the ventilation process cannot reach the pool zone directly. If this speculation is true, the Rhines–Young pool will be the least sensitive region to both surface wind and buoyancy flux variation.

f. *Relevance to observations*

Observations have shown clearly different thermocline variability features in different regions, as most clearly by Deser et al. (1996) in the North Pacific. From late 1976 to 1988, a prominent decade-long climate variability occurred in the upper thermocline temperature with a cooling in the central and western North Pacific, and a warming along the west coast of the North America. Why is the variability different in different regions? Is it caused by different surface forcings or by the different internal dynamics in the thermocline itself? These fundamental questions remain poorly understood. In this paper, the possible role of different thermocline dynamics in generating different variability features among different regions was investigated. However, to explain the observations, a more complete model is needed, which is under current investigation.

The identification and understanding of the geographic characteristics of the thermocline variability is undoubtedly important for our future study of the ocean circulation, particularly its long-term variability. This understanding will provide a sound physical basis for the interpretation of climatological oceanic data, and for the design of future long-term field experiments as well as GCM experiments and climate studies.

Acknowledgments. The work is supported by the Physical Oceanography Program (OCE-9401599), Climate Dynamics Program (ATM-9302884) of NSF, and Young Investigator Award of ONR. The author thanks Dr. W. R. Holland for providing the eddy-resolving, multilayer QG model used in the discussion in section 4. The author also thanks the three anonymous reviewers for their helpful comments.

REFERENCES

Anderson, D. L. T., and A. E. Gill, 1975: Spin-up of a stratified ocean, with applications to upwelling. *Deep-Sea Res.*, **22,** 583–596.

Antonov, J. I., 1993: Linear trends of temperature at interdecade and deep layers of the North Atlantic and the North Pacific Oceans: 1957–1981. *J. Climate,* **6,** 1928–1942.

Deser, C., and M. L. Blackmon, 1993: Surface climate variations over the North Atlantic Ocean during winter: 1900–1989. *J. Climate,* **6,** 1743–1753.

——, M. A. Alexander, and M. S. Timlin, 1996: Upper-ocean thermal variations in the North Pacific during 1970–1991. *J. Climate,* **9,** 1840–1855.

Dewar, W., 1989: A theory of time-dependent thermocline. *J. Mar. Res.,* **47,** 1–31.

Emery, W. J., and L. Magaard, 1976: Baroclinic Rossby waves as inferred from temperature fluctuations in the Eastern Pacific. *J. Mar. Res.,* **34,** 365–385.

Holland, W., and P. Rhines, 1980: An example of eddy-induced ocean circulation. *J. Phys. Oceanogr.,* **10,** 1010–1031.

Kushnir, Y., 1994: Interdecadal variations in North Atlantic sea surface temperature and associated atmospheric conditions. *J. Climate,* **7,** 141–157.

Levitus, S., 1988: Ekman volume fluxes for the World Ocean and individual ocean basins. *J. Phys. Oceanogr.,* **18,** 274–279.

Liu, Z., 1993a: Thermocline forced by varying wind. Part I: Spin-up and spin-down. *J. Phys. Oceanogr.,* **23,** 2505–2522.

——, 1993b: Thermocline forced by varying wind. Part II: Annual and decadal Ekman pumping. *J. Phys. Oceanogr.,* **23,** 2523–2540.

——, 1996: On the destruction of inertial recirculation by annual wind migration. *J. Phys. Oceanogr.,* **26,** 242–256.

——, and J. Pedlosky, 1994: Thermocline forced by annual and decadal surface temperature variation. *J. Phys. Oceanogr.,* **24,** 587–608.

Luyten, J., J. Pedlosky, and H. Stommel, 1983: The ventilated thermocline. *J. Phys. Oceanogr.,* **13,** 292–309.

Marshall, J., 1984: Eddy–mean flow interaction in a barotropic ocean model. *Quart. J. Roy. Meteor. Soc.,* **110,** 573–590.

Mysak, L. A., 1983: Generation of annual Rossby waves in the North Pacific. *J. Phys. Oceanogr.,* **13,** 1908–1923.

Price, J. M., and L. Magaard, 1980: Rossby wave analysis of the baroclinic potential energy in the upper 500 meters of the North Pacific. *J. Mar. Res.,* **38,** 249–264.

——, and ——, 1983: Rossby wave analysis of subsurface temperature fluctuations along the Honolulu–San Francisco great circle. *J. Phys. Oceanogr.,* **13,** 258–268.

——, and ——, 1986: Interannual baroclinic Rossby waves in the midlatitude North Atlantic. *J. Phys. Oceanogr.,* **16,** 2061–2070.

Qiu, B., and T. Joyce, 1992: Interannual variability in the mid- and low-latitude western North Pacific. *J. Phys. Oceanogr.,* **22,** 1062–1079.

Rhines, P., and W. R. Young, 1982: A theory of the wind-driven circulation. Part I: Mid-ocean gyres. *J. Mar. Res.,* **40** (Suppl.), 559–596.

Roemmich, D., and C. Wunsch, 1984: Apparent changes in the climatic state of the deep North Atlantic Ocean. *Nature,* **307,** 447–450.

Tabara, B., B. Thomas, and D. Ramsden, 1986: Annual and interannual variability of steric sea level along line *P* in the Northeast Pacific Ocean. *J. Phys. Oceanogr.,* **16,** 1378–1398.

Talley, L. D., and W. B. White, 1987: Estimates of time and space scales at 300 meters in the midlatitude North Pacific from TRAMSPAC XBT program. *J. Phys. Oceanogr.,* **17,** 2168–2188.

White, W., and S. Tabara, 1987: Interannual westward-propagating baroclinic long-wave activity on line *P* in the eastern Midlatitude North Pacific. *J. Phys. Oceanogr.,* **17,** 385–396.